KSCE Journal of Civil Engineering 29 (2025) 100205

Contents lists available at ScienceDirect

KSCE Journal of Civil Engineering

journal homepage: www.elsevier.com/locate/kscej

Dynamic behaviour analyses for a pile-supported structure with a MLS through 1g shaking table tests

Jungwon Yun [a,*], Geongsu Park [b], Byungmin Kim [c], Jintae Han [d]

[a] Land and Housing Research Institute, Daejeon 34047, Korea
[b] Dept. of Electrical Engineering, Korea Army Academy at Yeongcheon, Yeongcheon 38900, Korea
[c] Dept. of Urban and Environmental Engineering, Ulsan National Institute of Science and Technology, Ulsan 44919, Korea
[d] Dept. of Geotechnical Engineering, Korea Institute of Civil Engineering and Building Technology, Gyeonggi 10223, Korea

ARTICLE INFO

Keywords:
1g shaking table test
Magnetic levitation system
Pile-supported structure
Seismic performance

ABSTRACT

In this study, 1g shaking table tests were conducted to evaluate the seismic performance of a pile-supported structure incorporating a magnetic levitation system (MLS). The MLS was designed by installing electromagnets on the pile caps and permanent magnets on the underside of the deck. First, frequency sweep tests were conducted to determine the natural frequency of the MLS, confirming a significant isolation effect when the MLS was applied. Next, the acceleration phase characteristics with the application of MLS were analyzed. The results showed that the proposed MLS incurs a slight increase in response at long-period range but a significant decrease in response within the short-period range, which has a substantial impact on the structural behaviour. This indicates improvement in seismic stability performance, particularly in mitigating risks during critical-period events.

1. Introduction

In the event of an earthquake, excessive stress may be concentrated in the pile caps of a pile-supported structure. Therefore, researchers have consistently attempted to enhance seismic performance by installing isolation systems at the pile caps and superstructure connections. the performance of rubber isolation systems applied to pile caps has been validated (OS Kwon et al., 2002, OS Kwon et al., 2002). It has been observed that the application of a rubber isolation system to the pile caps reduces the response acceleration, as the natural period of the entire structure increases. In addition, the seismic performance of structures has been evaluated by installing friction- and roller-type isolation systems on piles or bridge caps (Eröz & DesRoches, 2008; Lin P. Y. & Lin T. K., 2012; Zheng et al., 2021; Yun et al., 2023). In 2023, Yun et al. indicated that roller-type isolation systems exhibit better performance in terms of acceleration response than friction-type systems but cautioned that such systems could incur long-period resonance.

However, conventional seismic isolation systems are typically installed between physically connected piles and structures, making it challenging to achieve the desired seismic performance during earthquakes. Accordingly, recent studies have been conducted on magnetic levitation-based seismic systems that can overcome the limitations of conventional seismic systems by completely floating structures (Rohmanuddin et al., 2011; Robertson, 2013; Amarante dos Santos & Fraternali, 2022).

A magnetic levitation system employs a mechanism that lifts structures by generating a magnetic force in the repulsion direction, typically achieved through an arrangement of permanent magnets or electromagnets. In 2010, Sasaki et al. conducted a study to improve the damping effect in a superconducting seismic isolation device (Sasaki et al., 2010a). Their findings indicated that vibration of permanent magnets during earthquakes induces eddy currents in metal structures, enhancing damping characteristics. Researchers have also explored improving lifting performance by directing the magnetic field into a specific direction through the geometric arrangement of multiple permanent magnets, known as a Halbach array (Sasaki et al., 2010b).

The aforementioned studies focused on structures utilizing permanent magnets for levitation. The addition of electromagnets to magnetic levitation systems for advanced vibration control has also been explored (Peijnenburg, 2006). An advantage of electromagnets over permanent magnetic is the ability to adjust the magnetic force by varying the voltage applied to them, facilitating the attainment of specific response characteristics by system designers. In 2013, Robertson developed a levitation system combining a permanent magnet set and an electromagnet-permanent magnet set. In 2014, Kamel et al. (2014)

* Corresponding author.
E-mail addresses: 92creative@naver.com (J. Yun), gsparkarmy1324@gmail.com (G. Park), byungmin.kim@unist.ac.kr (B. Kim), jimmyhan@kict.re.kr (J. Han).

https://doi.org/10.1016/j.kscej.2025.100205
Received 21 October 2024; Received in revised form 20 February 2025; Accepted 21 February 2025
Available online 24 February 2025

Nomenclature

MLS	Magnetic levitation system
PM	Permanent magnet
EM	Electromagnet
B	Magnetic flux density
J	Electric current density
U	Magnetic potential energy of a dipole
G	Gravitational constant
M_E	Mass of the earth
m_i	Mass of the isolation system
k_{spr}	Spring constant
λ	Scaling factor (prototype/model)
EI	Flexural rigidity
EA	Axial rigidity
USCS	Unified soil classification system
SP	Poor sand
C_g	Coefficient of curvature
C_u	Coefficient of uniformity
G_s	Specific gravity of soil
$\gamma_{d.\ max}$	Maximum dry unit weight
$\gamma_{d.\ min}$	Minimum dry unit weight
β	Coefficient for determining the location of the virtual fixed-point
N	Average N-value of the ground by standard penetration testing
k_h	Coefficient of the horizontal subgrade reaction
D	Pile diameter
L	Length from the pile cap to the virtual fixed point
K	Horizontal stiffness of the pile
T	Natural period of the system
FFT	Fast Fourier transform
ϕ	Acceleration phase difference (in radians)
t_M	Time at which the peak model response occurs
t_I	Time at which the peak input response occurs
ARR	Acceleration response ratio
SDRS	Standard design response spectrum

analyses the dynamic model of a vertically arranged electromagnet and permanent magnet isolation system, evaluating its vibration isolation performance under known disturbances. In 2020, Xu et al. (2020) devised a magnetic levitation system combining electromagnets and permanent magnets using an equivalent magnetic circuit model. They confirmed that the repulsive force between the electromagnet and permanent magnet is proportional to the square of the current applied to the electromagnet.

Electromagnets offer the further advantage of controlling the magnetic force by adjusting the applied voltage and current. In addition, an electromagnet enables active feedback control (Castellanos et al. 2018). In 2020, Yipeng et al. (2020) applied sliding mode control to a magnetic levitation system with a synchronous motor, using fuzzy logic for cancelling unknown disturbances. In 2020, Jiang and Ueno (2020) developed a magnetic levitation (maglev) system consisting of circularly arranged magnets. They suggested using a nonlinear rotational dynamic equation model and sliding-mode nonlinear controller to control the position and tilt angle of the structure. Such an active feedback control system has also been used to enhance the performance of seismic levitation systems compared to conventional permanent-magnet-based passive levitation systems (Chamraz et al., 2021).

Most of the aforementioned studies primarily focused on the development and precise control of the magnetic levitation system themselves. There has been a notable absence of research on evaluating the applicability of these devices when installed and implemented in structures. As mentioned previously, in pile-supported structures, excessive stress concentration in the pile caps can lead to structural damage. Therefore, applying a magnetic levitation system to the pile caps could effectively enhance the performance and reduce the risk of damage caused by excessive stress.

In this study, a magnetic levitation system was implemented by installing electromagnets on the pile caps and permanent magnets on the underside of the deck of a pile-supported structure system. The system was then subjected to 1g shaking table tests, followed by an evaluation of the seismic performance of the pile-supported structure using a fabricated isolation system.

2. Materials and methods

2.1. Magnetic levitation system

A magnetic levitation system is a device that uses magnetic forces generated by permanent magnets or electromagnets to repel each other, thereby lifting a structure. When an electromagnet receives sufficient power, it creates a magnetic field similar to that of a permanent magnet. This magnetic field interacts with others generated by additional magnets, resulting in reciprocal force exchange. By adjusting the strength of the magnetic field produced by the electromagnet, the permanent magnet can be lifted vertically. Fig. 1 (Yadav et al., 2013) illustrates a typical magnet levitation system and the magnetic fields it generates.

However, in the aforementioned configuration it is not possible to ensure stability in the horizontal direction, as summarized by Earnshaw's theorem (Reusch, 1994). According to Maxwell's equations for electromagnetic fields, the divergence of the magnetic flux density B is zero:

$$\nabla \cdot B = 0 \tag{1}$$

Using the vector triple product, Eq. (1) can be written as

$$\nabla \times (\nabla \times B) = \nabla(\nabla \cdot B) - (\nabla \cdot \nabla)B = -\nabla^2 B \tag{2}$$

According to the fundamental postulates of magneto-statics in free space,

$$\nabla \times B = \mu_0 J \tag{3}$$

Where μ_0 is the permeability of the free space, $\mu_0 = 4\pi \times 10^{-7}\ [H/m]$, and J is the current density. Substituting Eq. (3) into Eq. (2) yields

$$\nabla^2 B = -\mu_0 \nabla \times J \tag{4}$$

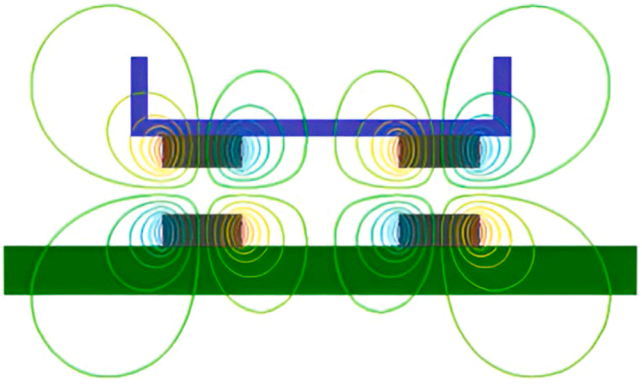

Fig. 1. Typical magnetic levitation system and the magnetic fields (front view).

If the effective volume is defined as the space in which the pile-supported structure on the magnetic levitation system can move, the current density, J, inside the effective space becomes zero. Although current is applied to the electromagnetic pairs, they are located outside the effective volume. This implies

$$\nabla^2 B = 0 \tag{5}$$

In addition, the magnetic potential energy of a dipole, U is given by

$$U = -M \cdot B \tag{6}$$

Assuming that the magnetic dipole moment of the permanent magnet, M, is time invariant, (5) can be rewritten as

$$\nabla^2 U = \frac{\partial^2 U_x}{\partial x^2} + \frac{\partial^2 U_y}{\partial y} + \frac{\partial^2 U_z}{\partial z^2} = 0 \tag{7}$$

For this system to be stable, the second derivative of the magnetic potential energy must be greater than zero along each axis, and the system must approach local (or global) minimum. However, according to 7, there is no local minimum point in the magnetic field; only the saddle point has a different sign for the second derivatives along each axis. This saddle point can be represented as shown in Fig. 2.

In the case of the above system, at the equilibrium point where the vertical magnetic force from the electromagnetic and gravitational forces acting on the deck balance each other, the system is stable along the vertical axis but unstable in the horizontal direction, even for small disturbances.

However, stability in the horizontal direction can also be achieved by adding a spring. In the absence of a spring, the potential energy due to magnetic force and gravitational force can be expressed as follow.

$$U = -M \cdot B - G\frac{M_E m_i}{z} \tag{8}$$

Where G is gravitational constant, M_E is mass of the earth, and m_i is mass of the isolation system, respectively. When the elastic energy due to the spring is added, the total potential energy can be expressed by 9, using the stiffness of spring, k_{spr} and displacement from the equilibrium point.

$$U = -M \cdot B - G\frac{M_E m_i}{z} + \frac{1}{2}k_{spr}\left(x^2 + y + z^2\right) \tag{9}$$

The second derivative of the total potential energy, as shown in 9, ensures stability in each axis by adding a spring with an appropriate spring stiffness, k_{spr}.

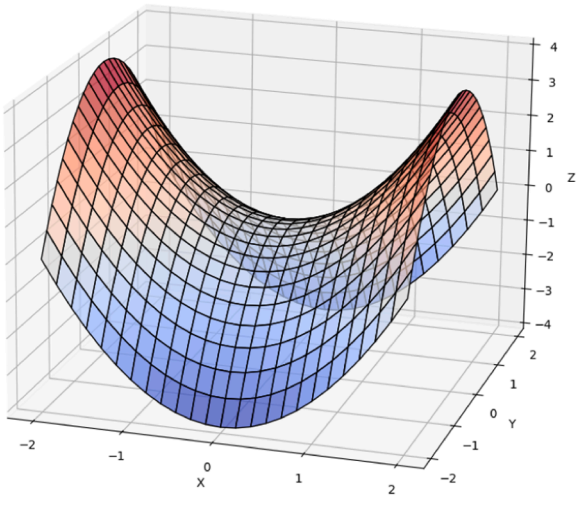

Fig. 2. Ball in unstable equilibrium on a saddle-shaped curve.

$$\nabla^2 U = -2G\frac{M_E m_i}{z^3} + 3k_{spr} > 0 \tag{10}$$

Therefore, springs were installed in this study, as shown in Fig. 3. The stiffness of each installed spring was 0.18 kN/m, and eight springs were installed to generate horizontal restoring forces. Figs. 3(a) and (b) illustrate the front and plan views, respectively, of the magnetic levitation system developed in this study. Electromagnets were installed on the upper part of each pile, and permanent magnets were installed under the deck. A plastic structure was placed between the electromagnet and permanent magnet, preventing direct connection and allowing the deck to be lifted vertically. A horizontal displacement of approximately 20 mm was ensured, and in the event of such displacement, the springs installed between the deck and plastic structure provided restoring forces. The specifications of the magnetic levitation system are listed in Table 1.

2.2. 1g shaking table model test

1g shaking table model tests are experimental techniques that scale down a prototype structure according to similarity laws to replicate its behaviour. This system is widely used to evaluate the seismic performance of seismic isolation systems (Calhoun & Harvey Jr, 2018; Yun et al., 2023). The soil box used in this study was fabricated from acrylic and measured 82 cm in length, 82 cm in width, and 68 cm in height (Fig. 4). To minimize interference from reflected waves during shaking, 5 cm thick sponges were attached to both walls (Lim & Jeong, 2018; Yun et al., 2023).

A 2 × 2 pile group was chosen as the experimental model based on a pile-supported structure in Pohang, South Korea. The experimental model was constructed at a 1/24.5 scale following similarity laws proposed by Iai in 1989 (Table 2). The similarity laws for the flexural rigidity (EI) of the pile were satisfied to appropriately simulate its lateral behavior (Yun & Han, 2021; Yun & Han, 2023). Additionally, similarity laws were applied to match the upper mass of the model (including the electromagnet, permanent magnet, and deck) with the mass of the prototype. The pile tip was fixed to the bottom of the soil box to simulate an end-bearing pile, with a total length of 50 cm and an embedded depth of approximately 40 cm into the soil. The properties of the model structure are detailed in Table 3.

The ground was simplified as a horizontal ground with a relative density of 90 % to prevent settlement during shaking. To achieve a relative density of 90 %, sinusoidal motions with a frequency of 10 Hz and an amplitude of 0.4 g were applied for 1 min at 10-cm intervals. Dry Jumunjin sand was used in this study; its properties are listed in Table 4. According to the Unified Soil Classification System (USCS), the sand is classified as poor sand (SP).

Acceleration and laser displacement meters were installed to measure the acceleration and displacement of the system. Fig. 4 shows the layouts and instrumentation locations of the fixed pile head model and the isolation system model with the magnetic levitation system. Fig. 5 displays the experimental photographs taken before and after operating the magnetic levitation system in the isolation system model.

The input seismic motions used in the experiment were sinusoidal motions with easily adjustable frequency and acceleration amplitude. This study focused on analyzing the structural response based on the frequency characteristics of the input motion and the acceleration phase relationship. Therefore, compared to actual seismic motions, which exhibit complex characteristics, the use of sinusoidal motions with adjustable frequency was deemed appropriate. In this study, a total of 52 tests were conducted. First, a frequency sweep test was performed in the range of 0.5 to 15 Hz to determine the natural frequencies. Subsequently, incremental tests were conducted to increase the seismic acceleration amplitude from 0.03 to 0.17 g. These tests were performed at frequencies of 2, 4, 6, 8, and 10 Hz. The maximum acceleration level of 0.17g was determined at a level that does not cause damage to the pile,

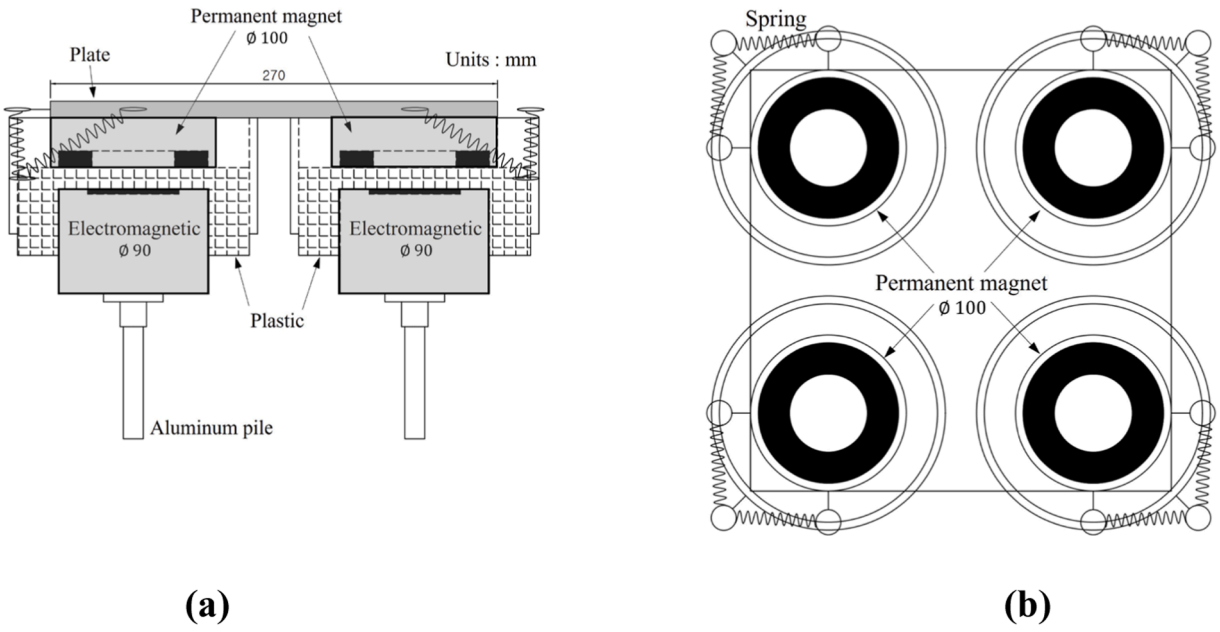

Fig. 3. Magnetic levitation system (in model scale). (a) Front view. (b) Plan view.

Table 1
Specification of magnetic levitation system.

Variable	Value	Unit	Description
Dimensions (electromagnet)	63 × 90 Φ	mm	Size of electromagnet
Dimensions (permanent magnet)	9.5 × 100 Φ	mm	Size of permanent magnet
Input voltage	0–100	VDC	Adjustable using hand-knob
Max. current output	10	A	
Max. force	6	kgf	With a set of permanent magnets

and the frequency range was selected based on the natural frequency of the structure. Details of the input accelerations used in the experiment are provided in Table 5.

3. Results

Typically, the inertial forces that strongly affect a structure's behaviour are calculated based on its acceleration amplitude and mass. Furthermore, these inertial forces can increase significantly when resonance occurs in the structure. Therefore, this study focused on analysing the acceleration response and determining the natural frequencies of the system.

In this section, the natural frequencies of each model are theoretically calculated using the virtual fixed-point method, which closely approximate the actual structural stiffness and inertial forces. This method is widely used in the design of pile-supported structures and assumes a fixed point located at a distance of $1/\beta$ from the ground surface (Yun et al., 2022). Here, β is derived by assuming that the pile head reaction and bending moment are equal to those of a both-end-fixed boundary condition. Eq. (11) and (12) can be utilized to determine the value of β:

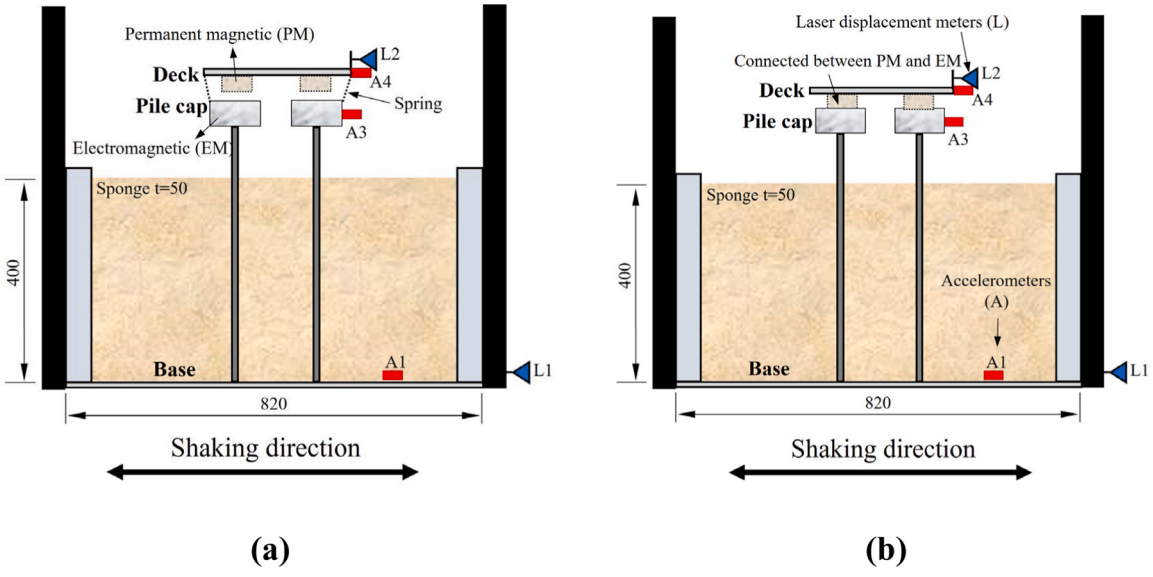

Fig. 4. Layouts of the 1g shaking table testing model (in model scale) with (a) the fixed pile head model and (b) the isolation system model (unit : mm).

Table 2
Scaling factors (λ = prototype/model) for 1g shaking table tests (Iai, 1989).

Quantity	Length	Density	Time	Acceleration	Velocity
Scaling factors	λ	1	$\lambda^{0.5}$	1	$\lambda^{0.5}$

Quantity	Displacement	Stress	Strain	Pore pressure	Stiffness
Scaling factors	λ	λ	λ	λ	λ

Quantity	Flexural rigidity (EI)	Axial rigidity (EA)	Moment	Shear force	Axial force
Scaling factors	λ^5	λ^3	λ^4	λ^3	λ^3

Table 3
Properties of pile-supported structure models.

Pile Diameter (mm)	Thickness (mm)	Length (mm)	Density ($kN{\cdot}m^{-3}$)	Flexural rigidity ($kN{\cdot}m^2$)
14	2	500	26.4	9.5×10^{-2}

Deck plate	Permanent magnetic system		Electromagnetic system	
Thickness (mm)	Density ($kN{\cdot}m^{-3}$)	Weight (N)	Weight (N)	Weight (N)
10.6	26.4	19.8	24.5	113.1

Table 4
Properties of Jumunjin sand.

Unified Soil Classification System (USCS)	Coefficient of curvature (C_g)	Coefficient of uniformity (C_u)	Specific gravity of soil (G_s)	Max. dry unit weight ($\gamma_{d.max}$, $kN{\cdot}m^{-3}$)	Min. dry unit weight ($\gamma_{d.min}$, $kN{\cdot}m^{-3}$)
Poor sand (SP)	0.93	1.48	2.65	16.2	13.7

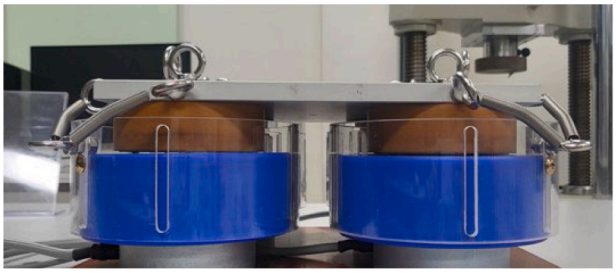

(a)

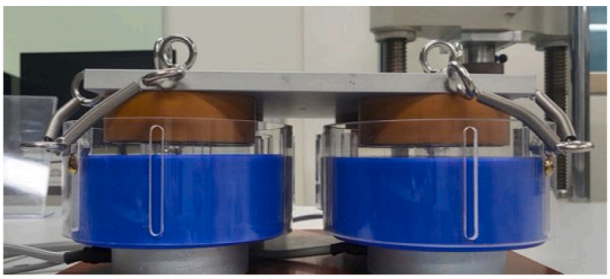

(b)

Fig. 5. Photos of the magnetic levitation system (a) before and (b) after the lifting action.

Table 5
Input seismic motion.

	Pile head conditions	Frequency (Hz)	Base acceleration amplitude (g)	Duration (s)
Frequency sweep tests	Isolated system model	0.5 – 15	0.1	30
	Fixed pile head model	0.5 – 15	0.1	30
Incremental tests	Isolated system model	2	0.03,0.06,0.09,0.12,0.15	10
		4	0.04,0.08,0.11,0.14,0.16	10
		6	0.04,0.07,0.10,0.13 0.17	10
		8	0.04,0.07,0.10,0.14,0.18	10
		10	0.03,0.07,0.10,0.14,0.17	10
	Fixed pile head model	2	0.03,0.06,0.09,0.12,0.15	10
		4	0.04,0.08,0.11,0.14,0.16	10
		6	0.04,0.07,0.10,0.13,0.17	10
		8	0.04,0.07,0.10,0.14,0.18	10
		10	0.03,0.07,0.10,0.14,0.17	10

$$\beta\ (cm^{-1}) = \sqrt[4]{\frac{k_h D}{4EI}} \tag{11}$$

$$k_h\ (kgf\,/\,cm^3) = 0.15N \tag{12}$$

where k_h is the coefficient of the horizontal subgrade reaction, D is the pile diameter, and EI is the flexural stiffness of the pile, N is the average N-value of the ground by standard penetration testing. N-value was converted using the Meyerhof (1956) equation based on the soil relative density derived from the shaking table tests.

Using the aforementioned equation, the length (L) from the pile cap to the virtual fixed point can be determined, and the horizontal stiffness (K) of the pile and natural period (T) of the system can be calculated using (13) and (14), respectively:

$$K\ (kgf\,/\,cm) = \Sigma\frac{12EI}{L^3}, \tag{13}$$

$$T\ (s) = 2\pi\sqrt{\frac{m}{K}}, \tag{14}$$

where m represents the mass of the deck plate.

The natural frequencies of the two experimental models were determined using the above equations. For the fixed pile head model, which integrates the permanent magnet (PM), electromagnet (EM), and deck, the overall mass was considered in calculating the natural frequency. However, for the isolation system model, where the EM and PM are separate, only the mass of the EM was used to calculate the natural frequency. The theoretical formulas yielded natural frequencies (on natural periods) of 8.8 Hz (0.11 s) for the fixed pile head model and 10.7 Hz (0.09 s) for the isolation system model. In the following section, the experimentally obtained natural frequencies will be calculated and compared with the theoretical results.

3.1. Frequency sweep test

Fig. 6 shows the acceleration response obtained from the frequency sweep test. Figures (a, c, e) illustrate the acceleration time history from the accelerometers installed on the structure, whereas figures (b, d, f) depict the acceleration amplitude ratio obtained through Fast Fourier Transform (FFT) analysis. Fig. 6(a) and (b) show the pile cap acceleration responses (A3) and amplitude ratios (A3/A1) of the fixed pile head model, respectively. Fig. 6(c) and (d) show the same responses for the isolation system model. Fig. 6(e) and (F) show the deck acceleration

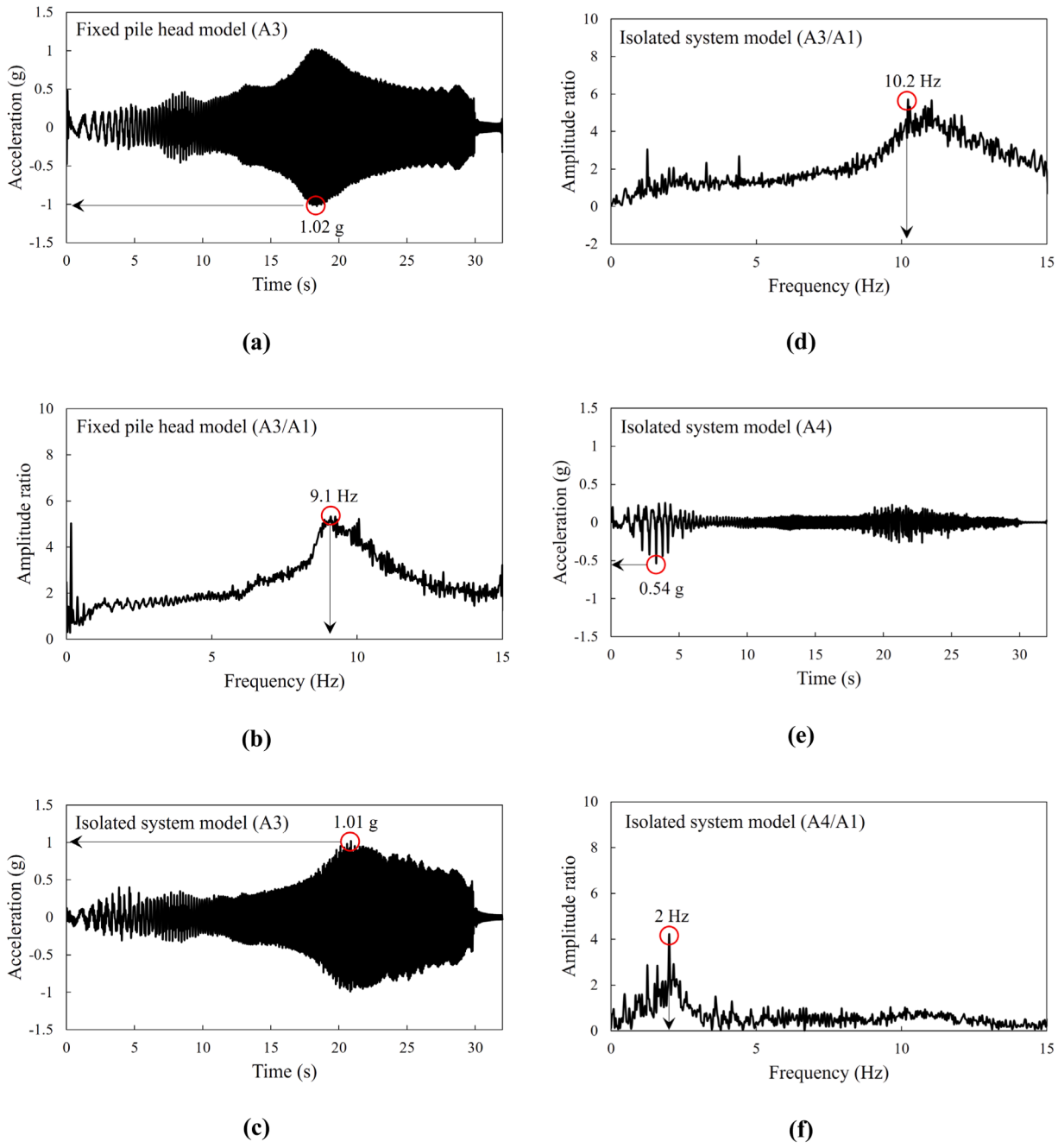

Fig. 6. Acceleration time history and FFT amplitude ratio during sweep tests. (a) Pile cap acceleration response (A3) and (b) FFT amplitude ratio (A3/A1) of fixed pile head model. (c) Pile cap acceleration response (A3) and (d) FFT amplitude ratio (A3/A1) of isolation system model. (e) Deck acceleration response (A4) and (f) FFT amplitude ratio (A4/A1) of the isolation system model (in model scale).

response (A4) and amplitude ratio (A4/A1) for the isolation system model.

Fig. 6(a) shows that the response gradually increased and peaked at 1.02 g around 18 s, followed by a gradual decrease. In the FFT result of Fig. 6(b), an amplification ratio of over 5 is observed at around 9.1 Hz, indicating that the largest response in the fixed pile head model occurred at the natural frequency of 9.1 Hz. This result closely corresponds to the theoretical natural frequency of 8.8 Hz obtained through calculations.

Fig. 6(c) presents the experimental results of the isolation system model with magnetic levitation. Similar to the findings in Fig. 6(a), the acceleration time history at the pile cap (A3) shows a continuous increase, reaching a peak of 1.01 g around 21 s before gradually decreasing. In the FFT results of Fig. 6(d), the maximum amplification ratio occurred at a higher frequency (10.2 Hz) compared to the fixed pile head model. This difference can be attributed to the isolation system's effect, which separates the pile cap and deck, reducing the mass supported by the pile. This finding closely matches the theoretical natural frequency of 10.7 Hz calculated.

Finally, Fig. 6(e) shows the acceleration response at the deck location (A4) of the isolation system model. The graph shows that the maximum response of 0.54 g occurred at approximately 3 s, and the natural frequency was determined to be 2 Hz, significantly lower than that of the pile cap response (Fig. 6(f)). This reduction can be attributed to the operation of the isolation system, which isolates the pile cap and deck. In such a system, the natural frequency is influenced by the stiffness of the spring and the mass of the deck. Additionally, a slight increase in the

response is observed around 20 s in Fig. 6(e). This phenomenon occurred because the pile cap and deck were connected by a spring, allowing energy transfer during resonance in the pile cap. However, due to the application of the magnetic levitation system, the maximum acceleration response at the deck was 47 % lower than that at the pile cap, demonstrating the effectiveness of the isolation system.

Thus, the natural frequencies for each model were approximately 10 Hz for the pile cap and approximately 2 Hz for the deck the isolation system was applied. To evaluate the behaviour of each model based on the natural frequency of the system, incremental tests were conducted by increasing the acceleration at the input frequencies of 2, 4, 6, 8, and 10 Hz.

3.2. Incremental test

3.2.1. Acceleration time history results according to the input frequency

Incremental tests were conducted to evaluate the model's behavior under varying input frequencies and input acceleration amplitudes. Fig. 7 illustrates the representative results of the experiments, where the model was subjected to the highest amplitude of acceleration (0.15–0.17 g) to evaluate its response across different input frequencies.

Figs. 7(a) and (b) show the responses of the fixed pile head and isolation system models, respectively, when subjected to an input frequency of 2 Hz. The accelerations of the pile cap in the two models increased by 38 and 20 %, respectively, compared to the base acceleration. This difference is attributed to the mass difference of the pile caps, which resulted in a more significant acceleration response in the fixed pile head model. In the isolation system model, the deck acceleration increased by approximately 30 % compared with the base acceleration. This can be explained by the resonance phenomenon occurring between the input frequency (2 Hz) and the natural frequency of the deck, as discussed earlier.

Next, Figs. 7(c) and (d) illustrate the responses of the fixed pile head and isolation system models, respectively, when subjected to an input

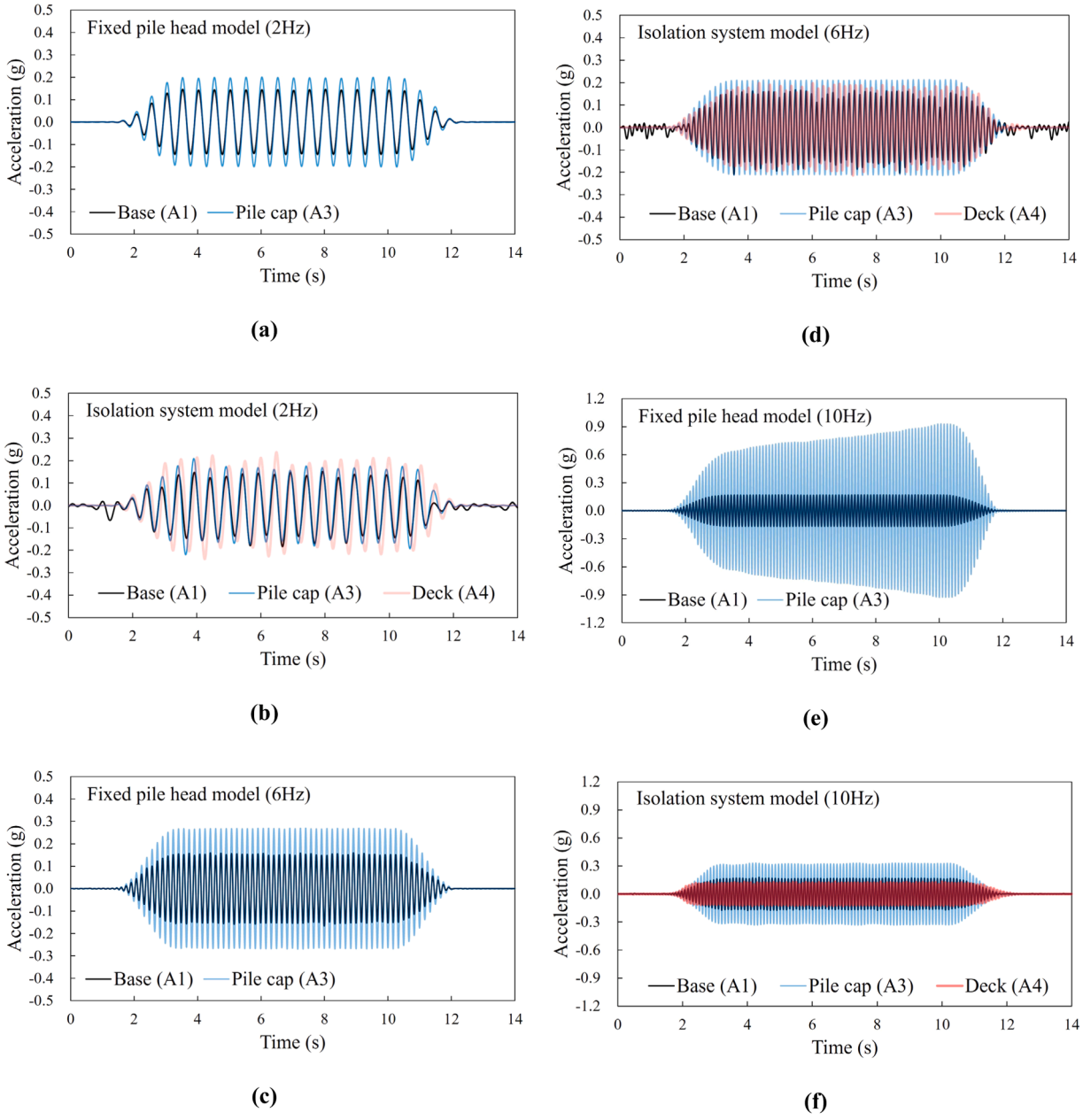

Fig. 7. Acceleration time history results according to input frequency. (a) Fixed pile head model (2 Hz). (b) Isolation system model (2 Hz). (c) Fixed pile head model (6 Hz). (d) Isolation system model (6 Hz). (e) Fixed pile head model (10 Hz). (f) Isolation system model (10 Hz) (in model scale).

frequency of 6 Hz. As depicted in Fig. 7(c), the pile cap acceleration increased by approximately 62 % compared with the base acceleration. This notable acceleration increase, compared to Fig. 7(a), is attributed to the input frequency of 6 Hz, which approaches the natural frequency of 9.1 Hz. However, as shown in Fig. 7(d), the differences in the acceleration between the base, pile cap, and deck were not significant. This is because, in the isolation system model, the input frequency of 6 Hz, natural frequency of the pile cap (10.2 Hz), and natural frequency of the deck (2 Hz) did not align, preventing resonance phenomena within the system.

Finally, Figs. 7(e) and (F) show the responses of the fixed pile head and isolation system models, respectively, when subjected to an input frequency of 10 Hz. In Fig. 7(e), the pile cap acceleration continues to rise, reaching a maximum increase of 350 % compared with the base acceleration. This is attributed to the close match between the input frequency (10 Hz) and natural frequency of the pile cap (9.1 Hz), leading to the resonance phenomenon and a continuous supply of energy. In contrast, Fig. 7(f) reveals that although the input frequency (10 Hz) aligns with the natural frequency of the pile cap (10.2 Hz), the pile cap acceleration increases by only 86 % compared with the base acceleration and does not show a continuous increase over time. Additionally, the deck acceleration decreases by approximately 23 % compared with the base acceleration. This is attributed to the different behavioral characteristics of the pile cap and deck, which led to a certain degree of mutual restraint in their behaviors. The acceleration phase characteristics should be analyzed based on the frequencies of the pile cap and deck to gain a clear understanding of the observed behavior.

3.2.2. *Acceleration phase relationship between the input motion and system*

The phase relationship between the input base motion and the system was analyzed based on the acceleration phase difference, with the results presented in Fig. 8. The figure depicts the magnified time region from 6 to 7 s of the acceleration time history of the isolation system model. To analyze the phase relationship, the peak points of each response were extracted, as shown in Fig. 8(a) (Tran et al., 2022; Yun & Han, 2024). Based on this, the phase difference between the input base motion and the system response was determined. Eq. (15) below illustrates the formula for determining the phase difference (ϕ):

$$\phi = 2\pi \frac{t_M - t_I}{T}, \tag{15}$$

where ϕ represents the acceleration phase difference (in radians), t_M represents the time at which the peak model response occurs, t_I represents the time at which the peak input acceleration occurs, and T represents the period of the input base motion. Fig. 9 illustrates the acceleration phase difference of the isolation system model, calculated using Eq. (8), according to the input frequency. Fig. 9(a) shows the phase difference between the input base motion (A1) and pile cap (A3), whereas Fig. 9(b) shows the phase difference between the input base motion (A1) and deck (A4).

Fig. 9(a) shows that the average phase differences of −8, 6, and 13° occur at 2, 6, and 10 Hz, respectively. The phase difference between the input motion and pile cap increased with the increasing frequency owing to the resulting increase in the phase difference between the input base motion and deck, as shown in Fig. 9(b). Consequently, the pile cap, which was connected to the deck by a spring, was influenced to some extent. However, Fig. 9(a) shows that the phase difference between the input base motion and pile cap remained below 20° across all frequency ranges. This is attributed to the experimental conditions, wherein the ground was highly compacted with a relative density of 90 %, indicating that the ground and pile behaved as an integrated system.

In Fig. 9(b), the phase difference is significantly higher than that in Fig. 9(a). At frequencies of 2, 6, and 10 Hz, average phase differences of 54, 85, and 159°, respectively, were recorded. The 2 Hz response in Figs. 8(a) and 9(b) shows that the phase difference between the input base motion and deck was in the range of 37–64°, which is a relatively small phase difference compared with the response at other frequencies. This is attributed to the resonance phenomenon occurring in the deck when the input frequency matched its natural frequency. Consequently, the input motion pushed the deck, leading to a small phase difference. Next, in the 6 Hz response in Figs. 8(b) and 9(b), the phase difference between the input base motion and the deck was determined to be in the range of 73–99°. Specifically, in Fig. 8(b), in the time domain where the maximum response occurs in the pile cap, the response of the deck is close to zero. Similarly, when the response of the deck is at its maximum, the pile cap response is close to zero. This suggests that, as explained earlier, resonance does not occur owing to the difference between the natural frequencies of the input base motion, pile cap, and deck.

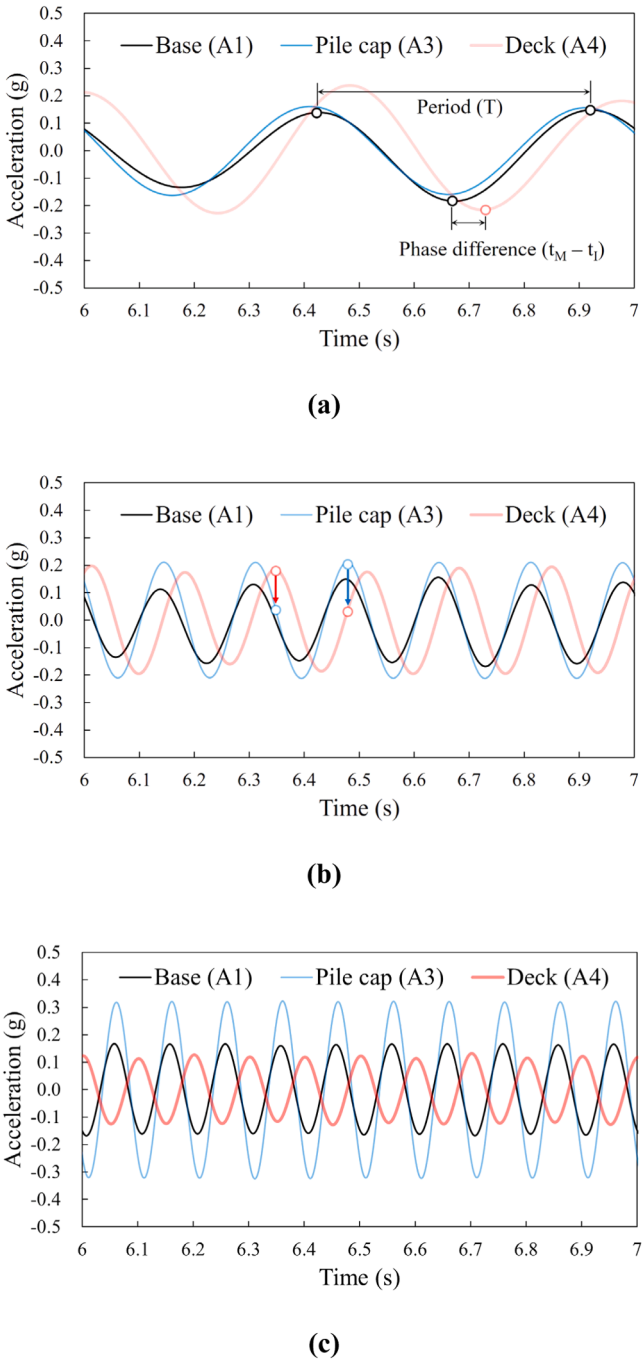

Fig. 8. Acceleration time history results of the isolation system model. (a) 2 Hz. (b) 6 Hz. (c) 10 Hz (in model scale).

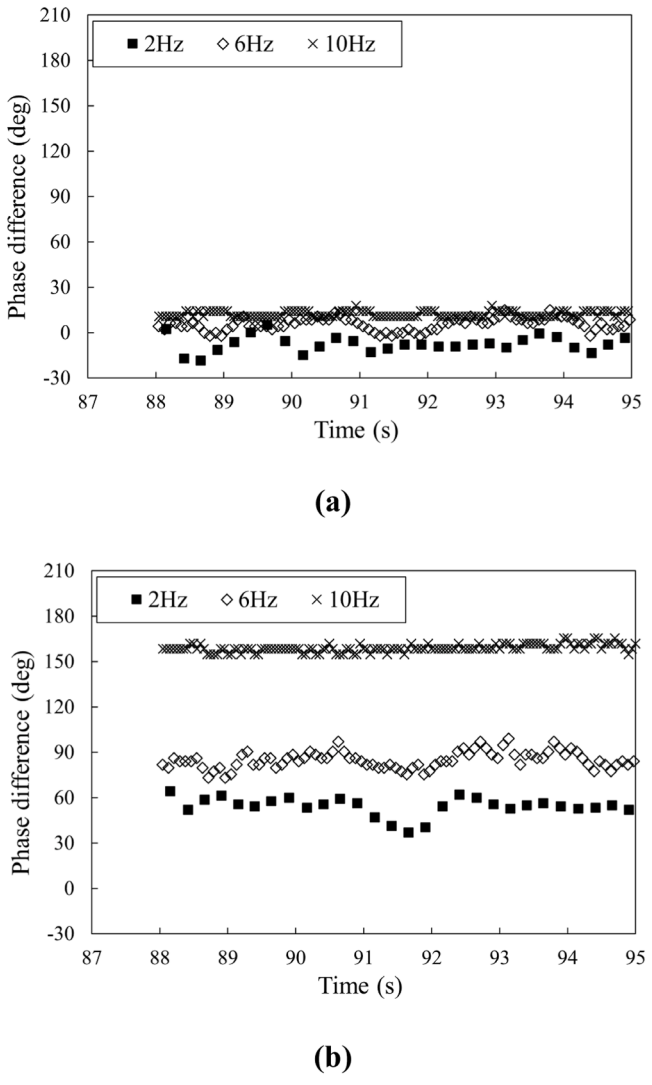

Fig. 9. Acceleration phase differences of the isolation system model. (a) Phase difference between input base motion (A1) and pile cap (A3). (b) Phase difference between input base motion (A1) and deck (A4). (in model scale).

Therefore, it can be concluded that none of components had significant influence on the other components' responses. Finally, in the 10 Hz response in Figs. 8(c) and 9(b), the phase difference between the input base motion and deck is determined to be in the range of 155–166°, indicating a phase in the opposite direction. This is attributed to the resonance occurring in the pile cap, as the input frequency matches the natural frequency of the pile cap. No resonance occurred in the deck at this frequency, allowing the deck to resist the behavior of the pile cap. Consequently, the pile cap response in Fig. 7(f) is significantly lower than that in Fig. 7(e).

Fig. 10 summarizes the aforementioned findings and illustrates the behaviour of the isolation system model. The figure depicts the arrows indicating the approximate direction and magnitude of acceleration. First, when the input motion frequency and natural frequency of the deck were similar, both the pile cap and deck exhibited similar phases, leading to an increase in the deck response. When the input motion frequency and natural frequencies of the pile cap and deck were different, the behaviour of the deck showed a phase difference of approximately 90° from that of the pile cap, with each component's response having little influence on the other's response. Finally, when the input base motion and natural frequency of the pile cap were similar, the behaviour of the deck showed an opposite phase to that of the pile cap, resulting in a decrease in both the pile cap and deck responses.

3.2.3. *Incremental test results according to the input base acceleration*

Fig. 11 shows the acceleration responses of the models based on the amplitude of the input base acceleration. Figs. 11(a)–(e) illustrate the acceleration responses of the fixed pile head and isolation system models when subjected to input frequencies ranging from 2 to 10 Hz. A review of each graph reveals that, up to an input acceleration of 0.06 g, the differences among the responses of the models are not significant (depicted in gray). This is attributed to the fact that, at low input accelerations, the inertial forces of the structure are not substantial, preventing resonance phenomena based on the natural frequencies of the structure. However, beyond an input acceleration of 0.06 g, substantial disparities in the response are observed. This study focused primarily on responses for input accelerations exceeding 0.06 g.

Fig. 11(a) shows the maximum acceleration response of the model subjected to an input frequency of 2 Hz. When the input acceleration exceeds 0.06 g, the upper deck (A4) of the isolation system model shows larger responses compared to the pile cap responses (A3). This occurrence is attributed to the resonance phenomenon caused by the alignment of the input frequency with the natural frequency of the deck, as explained earlier. By contrast, when the models are subjected to input frequencies of 4 Hz or higher the maximum response occurs at the pile cap (A3) of the fixed pile head model in all cases. This can be attributed to the integrated behavior of the pile cap and deck in the fixed pile head model, which influences the structural response. For the isolation system model, the response decreases significantly compared with that of the fixed pile head model. This is because of the phase difference caused by the disparity in the natural frequency between the pile cap and deck, as shown in Fig. 10.

Fig. 12 and Table 6 compare the acceleration response ratio (ARR) between the isolation system and fixed pile head models. In Fig. 12(a), the ARR is derived by dividing the pile cap acceleration (A3) of the

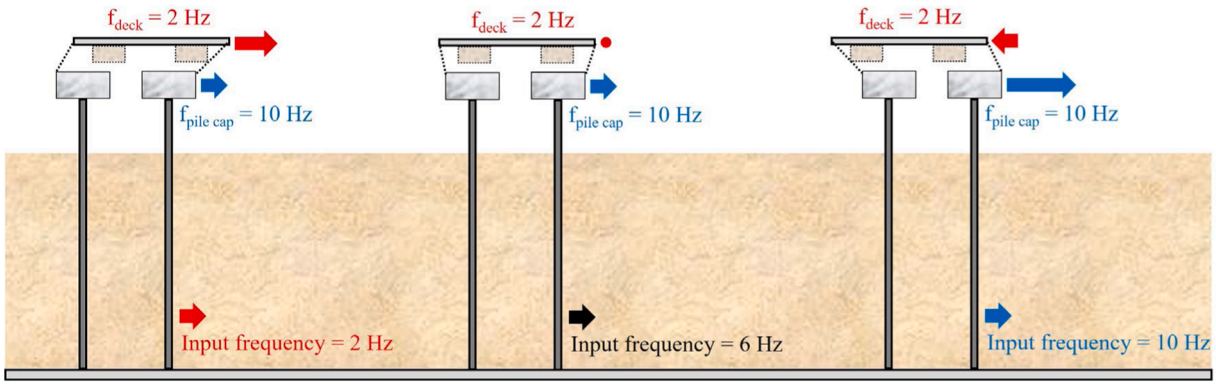

Fig. 10. Acceleration phase difference according to input frequency (in model scale).

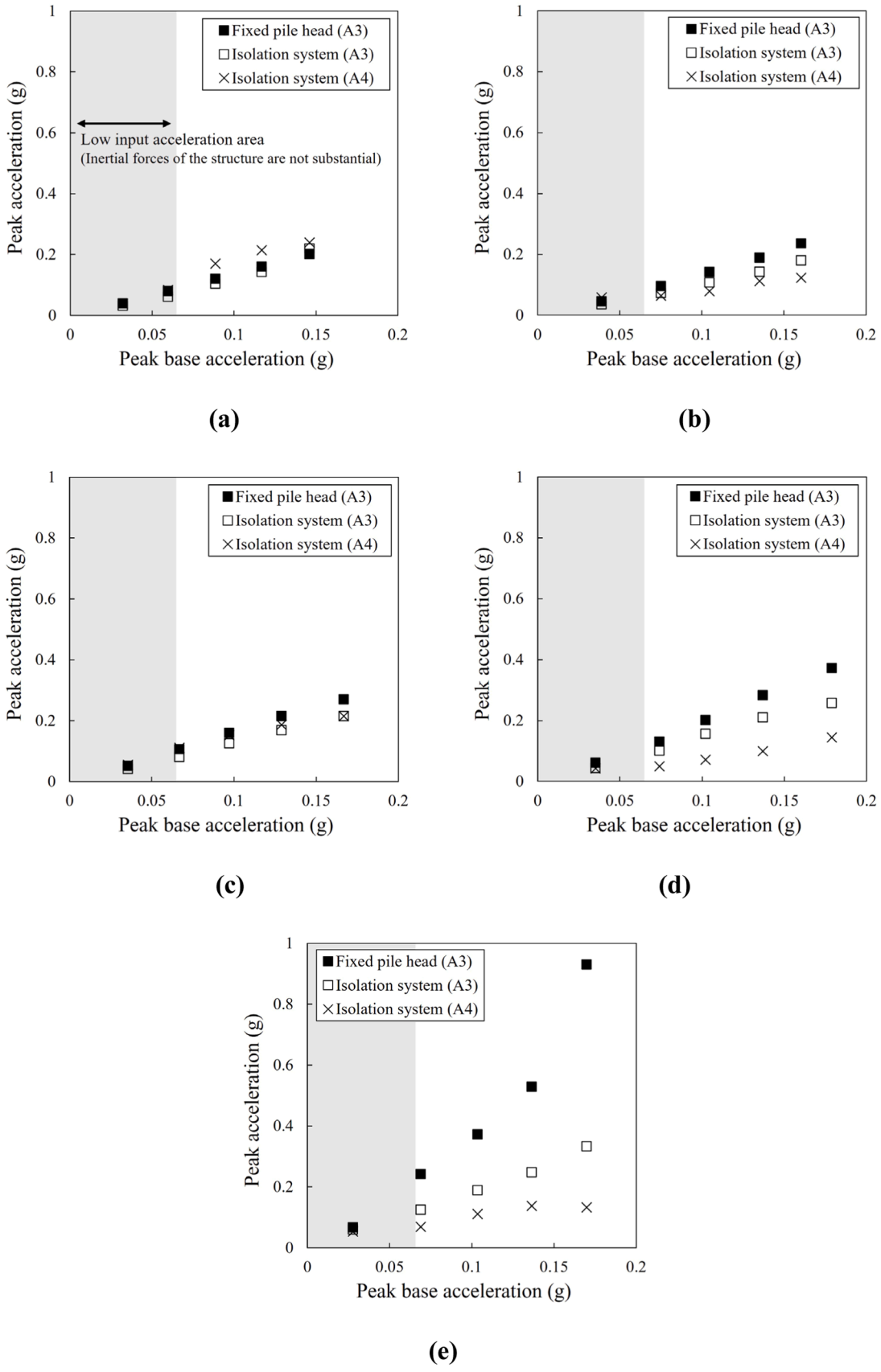

Fig. 11. Incremental test results according to input base acceleration. (a) 2 Hz. (b) 4 Hz. (c) 6 Hz. (d) 8 Hz. (e) 10 Hz (in model scale).

isolation system model by that of the fixed pile head model. Here, an ARR below 100 % indicates a reduction in the acceleration response due to the installation of a base isolation system. At input accelerations below 0.06 g, the ARR falls within the range of 72–90 %. As previously explained, this indicates that the inertial forces are relatively small and the response is not significantly influenced by the input frequency. In contrast, when the input acceleration exceeds 0.06 g, the response varies with the input frequency. The 2 Hz response shows that, as the input acceleration increases, the ARR also increases to within a range of 89–110 %. However, except at an acceleration of 0.15 g, the ARR is consistently below 100 %. In the 10 Hz response, the ARR decreases significantly with increasing input acceleration to within a range of 36–52 %. Finally, in the 4–8 Hz response, the ARR does not change substantially with the input acceleration, maintaining a range of 68–80 %.

Fig. 12(b) presents the results of deriving the ARR by dividing the

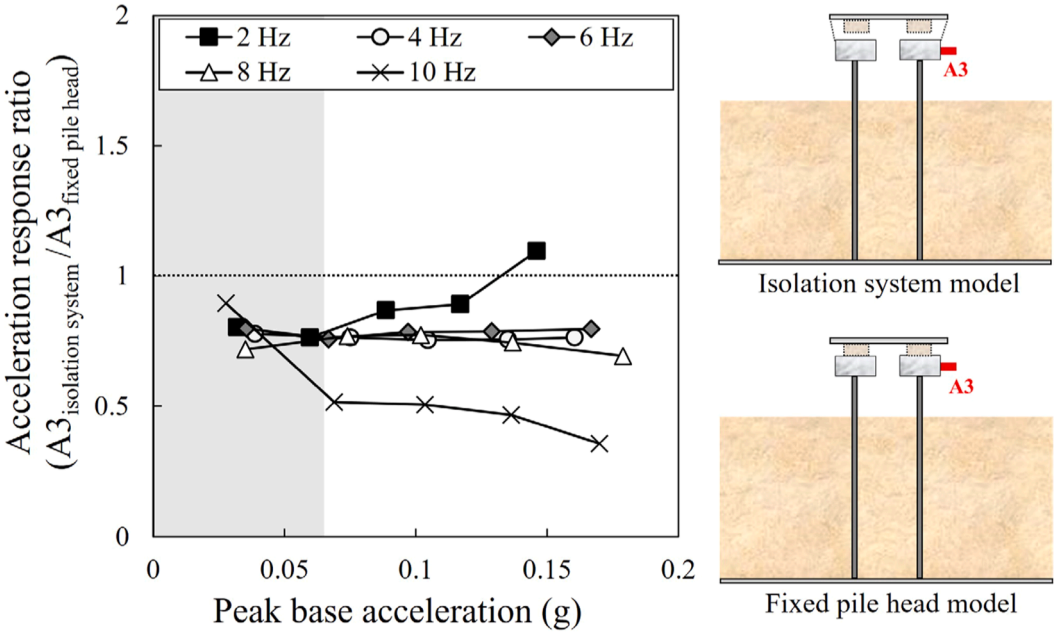

(a)

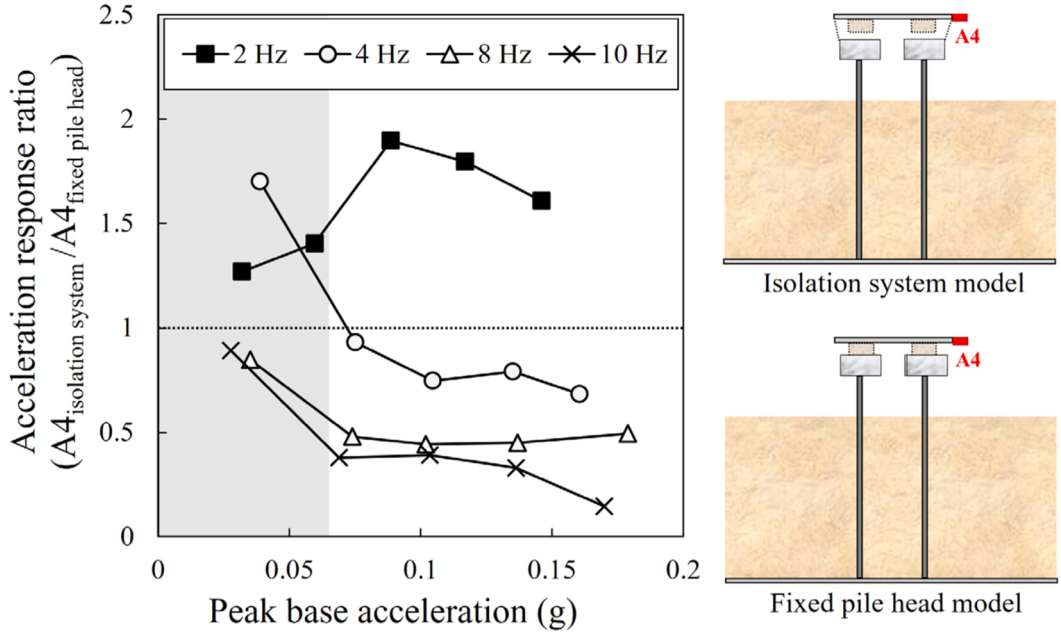

(b)

Fig. 12. Acceleration response ratio (ARR) between isolation system model and fixed pile head model. (a) ARR between isolation system model (A3) and fixed pile head model (A3). (b) ARR between isolation system model (A4) and fixed pile head model (A4) (in model scale).

Table 6
Acceleration response ratio (ARR) between isolation system model and fixed file head model.

ARR derivation location	Input frequency (Hz)	ARR according to input motion (Average ARR)
$\frac{A3_{isolation\ system}}{A3_{fixed\ pile\ head}}$	2	0.76, 0.87, 0.89, 1.1 (0.9)
	4	0.76, 0.75, 0.76, 0.76 (0.76)
	6	0.76, 0.78, 0.79, 0.8 (0.78)
	8	0.77, 0.77, 0.74, 0.69 (0.75)
	10	0.52, 0.51, 0.47, 0.36 (0.46)
$\frac{A4_{isolation\ system}}{A4_{fixed\ pile\ head}}$	2	1.4, 1.9, 1.8, 1.61 (1.68)
	4	0.93, 0.75, 0.79, 0.68 (0.79)
	6	–
	8	0.48, 0.44, 0.45, 0.49 (0.47)
	10	0.38, 0.39, 0.33, 0.15 (0.31)

deck acceleration (A4) of the isolation system model by the deck acceleration (A4) of the fixed pile head model. These two accelerations were compared to evaluate the reduction in the deck acceleration response when the isolation system was installed. This figure relates to cases where the input accelerations exceeded 0.06 g. The response at an input frequency of the deck at 2 Hz shows that the acceleration response increased by 61–90 %. However, as shown in Fig. 13(b), the 2 Hz frequency corresponds to the 2.5 s period on the prototype, indicating that the spectral acceleration does not appear to be large. At the natural frequency of 10 Hz of Fig. 12(b), the acceleration response of the deck decreased by 62–85 %. Finally, at 4–8 Hz, the acceleration response decreased by up to 56 %. At 6 Hz, however, accurate measurement was not possible due to measurement errors. In conclusion, the application of a magnetic levitation system resulted in decreased response across most natural frequency ranges, except at the natural frequency of the deck (2 Hz). Particularly notable was the reduction of up to 85 % in response at the natural frequency of the pile cap (10 Hz).

3.2.4. *Acceleration response spectrum results*

To examine the above from a seismic design perspective, we compared the standard design response spectrum (SDRS) with the structure response spectrum with ARR applied. Fig. 13 shows the SDRS corresponding to a 1000–year return period of S2 ground (shallow and dense) in South Korea, alongside the structure acceleration response with ARR applied to the SDRS. In the figure, the average ARR values from Table 6 are applied. This figure presents the experimental model response scaled to prototype conditions.

In Fig. 13(a), the pile cap acceleration response shows that the application of the magnetic levitation system decreases the acceleration response in most period ranges. However, Fig 13(b) depicting the deck acceleration response shows different results. The application of the magnetic levitation system increases the acceleration response by approximately 68 % in the 2.5 s range but decreases it by up to 69 % in the 0.5 s range. In the design response spectrum, there is a slight increase in response within the long–period range but a significant decrease within the short–period range, which has a substantial impact on the structural behavior. This indicates improvement in seismic performance, particularly in mitigating risks during critical–period events.

This study focused on evaluating the applicability of a magnetic levitation system to pile-supported structures. The results indicate promising outcomes, particularly in terms of reducing the acceleration responses. However, the experiments were conducted at a single ground condition. The behavior of a pile and structure can vary depending on the ground condition, necessitating future research under different ground conditions. Additionally, this study only used acceleration results to analyze the inertial forces affecting the behavior of the structure. However, the application of a magnetic levitation system to a pile cap can lead to significant displacement owing to the low spring stiffness at the connection. Therefore, future research considering the displacement

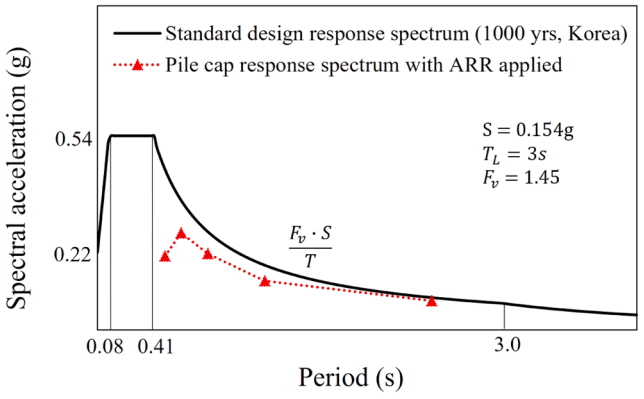

(a)

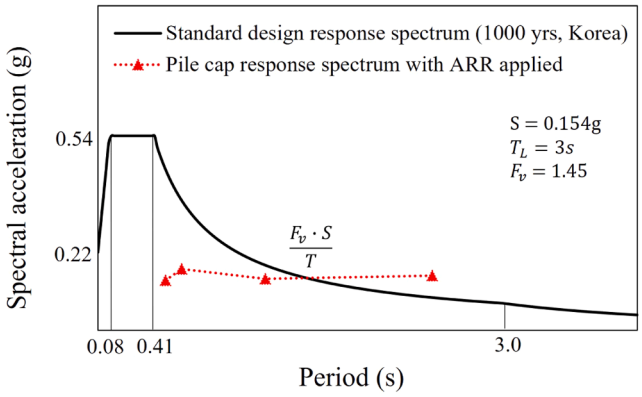

(b)

Fig. 13. Standard design response spectrum of Korea (1000-year return, S2 ground, MOF, 2017) and structure response spectrum with ARR applied. (a) Pile cap acceleration response (b) Deck acceleration response (in prototype scale).

responses in pile-supported structures with magnetic levitation systems applied to their pile caps is essential.

4. Conclusions

In this study, 1g shaking table tests were conducted to evaluate the seismic performance of a pile-supported structure with a magnetic levitation system. The magnetic levitation system was fabricated by installing an electromagnet onto the pile caps and a permanent magnet on the underside of the deck of the structure. First, frequency sweep tests were performed to determine the natural frequencies of the structure, followed by incremental tests to evaluate the behaviour of the model based on the input frequencies and acceleration amplitudes.

In the frequency sweep test, the natural frequencies and acceleration responses of each model were obtained. For the fixed pile-head model, the maximum acceleration response at the natural frequency of the pile cap (9.1 Hz) was found to be 1.02 g. For the isolation system model, the acceleration response at the natural frequency of the pile cap (10.2 Hz) was found to be 1.01g, whereas the acceleration response at the natural frequency of the deck (2 Hz) was found to be 0.54 g. This indicates a significant isolation effect when the magnetic levitation system is applied.

The acceleration phase characteristics relative to the input frequency

were analysed for the structure equipped with the magnetic levitation system. When the input base motion and the natural frequency of the deck were similar, both the pile cap and deck exhibited similar phases, leading to an increase in the deck response. When the natural frequencies of the input base motion, pile cap, and deck differed, the deck showed a phase difference of approximately 90° from the pile cap, indicating that the response of each component had little influence on the others. Finally, when the input base motion and natural frequency of the pile cap were similar, the deck exhibited an opposite phase to the pile cap, resulting in reduced deck responses.

The application of a magnetic levitation system increases the acceleration response of deck by approximately 68 % in the 2.5 s period but decreases it by up to 69 % in the 0.5 s period (at prototype scale). In the design response spectrum, there is a slight increase in response within the long–period range but a significant decrease in response within the short–period range, which significantly impacts structure behaviour. This improvement indicates enhanced seismic performance, particularly in mitigating risks during critical–period events.

CRediT authorship contribution statement

Jungwon Yun: Writing – original draft, Formal analysis, Data curation, Conceptualization. **Geongsu Park:** Writing – original draft, Data curation. **Byungmin Kim:** Conceptualization. **Jintae Han:** Conceptualization.

Declaration of competing interest

The authors declare that they have no known competing financial interests or personal relationships that could have appeared to influence the work reported in this paper.

Acknowledgements

This research was supported by a National Research Foundation of Korea (NRF) grant funded by the Korean Government (MSIT) (No. 2022R1F1A1071805).

References

Amarante dos Santos, F., & Fraternali, F. (2022). Novel magnetic levitation systems for the vibration control of lightweight structures and artworks. *Structural Control and Health Monitoring, 29*(8), E2973. https://doi.org/10.1002/stc.2973

Calhoun, S. J., & Harvey Jr, P. S. (2018). Enhancing the teaching of seismic isolation using additive manufacturing. *Engineering Structures, 167*, 494–503. https://doi.org/10.1016/j.engstruct.2018.03.084

Castellanos Molina, L. M., Galluzzi, R., Bonfitto, A., Tonoli, A., & Amati, N. (2018). Magnetic levitation control based on flux density and current measurement. *Applied Sciences, 8*(12), 2545. https://doi.org/10.3390/app8122545

Chamraz, Š., Huba, M., & Žáková, K. (2021). Stabilization of the magnetic levitation system. *Applied Sciences, 11*(21), 10369. https://doi.org/10.3390/app112110369

Eröz, M., & DesRoches, R. (2008). Bridge seismic response as a function of the Friction Pendulum System (FPS) modeling assumptions. *Engineering Structures, 30*(11), 3204–3212. https://doi.org/10.1016/j.engstruct.2008.04.032

Iai, S. (1989). Similitude for shaking table tests on soil-structure-fluid model in 1g gravitational field. *Soils and foundations, 29*(1), 105–118. https://doi.org/10.3208/sandf1972.29.105

Jiang, C., & Ueno, S. (2020). Study on vibration control system of structures based on magnetic levitation technology. *Mechanical Engineering Journal, 7*(1), 19–00307. https://doi.org/10.1299/mej.19-00307

Kamel, M., Kandil, A., El-Ganaini, W. A., & Eissa, M. (2014). Active vibration control of a nonlinear magnetic levitation system via Nonlinear Saturation Controller (NSC). *Nonlinear Dynamics, 77*, 605–619. https://doi.org/10.1007/s11071-014-1323-3

Kwon, O. S., Jang, I. S., & Park, W. S. (2002a). Evaluation and improvement of seismic performance of landing pier (I). *Korean Society of Civil Engineering, 22*(3–B), 353–363. In Korean.

Kwon, O. S., Jang, I. S., Park, W. S., & Cho, S. M. (2002b). Evaluation and improvement of seismic performance of landing pier (II). *Korean Society of Civil Engineers, 22*(4–B), 551–563. In Korean.

Lim, H., & Jeong, S. (2018). Simplified py curves under dynamic loading in dry sand. *Soil Dynamics and Earthquake Engineering, 113*, 101–111. https://doi.org/10.1016/j.soildyn.2018.05.017

Lin, P. Y., & Lin, T. K. (2012). Control of seismically isolated bridges by magnetorheological dampers and a rolling pendulum system. *Structural Control and Health Monitoring, 19*(2), 278–294. https://doi.org/10.1002/stc.431

Meyerhof, G. G. (1956). Penetration tests and bearing capacity of cohesionless soils. *Journal of the Soil Mechanics and Foundations Division, 82*(1), 1–19. https://doi.org/10.1061/jsfeaq.0000001

MOF. (2017). Design standards of harbour and port. Ministry of Oceans and Fisheries (MOF). *Sejong, Korea (in Korean)*.

Peijnenburg, A. T. A., Vermeulen, J. P. M., & Van Eijk, J. (2006). Magnetic levitation systems compared to conventional bearing systems. *Microelectronic engineering, 83*(4–9), 1372–1375. https://doi.org/10.1016/j.mee.2006.01.248

Reusch, M. F. (1994). A problem related to Earnshaw's theorem. *IEEE transactions on magnetics, 30*(3), 1324–1326. https://doi.org/10.1109/20.297771

Robertson, W. S. P. (2013). *Modelling and design of magnetic levitation systems for vibration isolation*. Adelaide, South Australia: University of Adelaide. PhD Thesis.

Rohmanuddin, M., Budi, E. M., & Purnama, R. (2011). In *Design of horizontal seismic sensor with spherical inverted pendulum and magnetic levitation*. IEEE. https://doi.org/10.1109/ICA.2011.6130156.

Sasaki, S., Shimada, K., Tsuda, M., Hamajima, T., Kawai, N., & Yasui, K. (2010a). Suitable structure of PM and copper plate systems for reducing vibration transmission and improving damping effect in a superconducting seismic isolation device. *IEEE transactions on applied superconductivity, 21*(3), 2233–2236. https://doi.org/10.1109/TASC.2010.2084062

Sasaki, S., Shimada, K., Yagai, T., Tsuda, M., Hamajima, T., Kawai, N., & Yasui, K. (2010b). Suitable shape and arrangement of HTS bulk and permanent magnet for improving levitation force in a magnetic levitation type superconducting seismic isolation device. *IEEE Transactions on Applied Superconductivity, 20*(3), 985–988. https://doi.org/10.1109/TASC.2010.2042159

Tran, N. X., Bong, T., & Kim, S. R. (2022). Kinematic and inertial interaction of single and group piles in slope by displacement phase relation. *Journal of Earthquake Engineering, 26*(7), 3639–3659. https://doi.org/10.1080/13632469.2020.1813661

Xu, J., Yang, X., Li, W., Zheng, J., Wang, Y., & Fan, M. (2020). Research on semi-active vibration isolation system based on electromagnetic spring. *Mechanics & Industry, 21*(1), 101. https://doi.org/10.1051/meca/2019048

Yadav, M., Mehta, N., Gupta, A., Chaudhary, A., & Mahindru, D. V. (2013). Review of magnetic levitation (maglev): A technology to propel vehicles with magnets. *Global Journal of Researches in Engineering Mechanical & Mechanics, 13*(7), 32–33.

Yipeng, L., Jie, L., Fengge, Z., & Ming, Z. (2020). Fuzzy sliding mode control of magnetic levitation system of controllable excitation linear synchronous motor. *IEEE Transactions on Industry Applications, 56*(5), 5585–5592. https://doi.org/10.1109/TIA.2020.3004763

Yun, J. W., Han, J. T., & Kim, J. (2022). Evaluation of the virtual fixed-point method for seismic design of pile-supported structures. *KSCE Journal of Civil Engineering, 26*(2), 596–605. https://doi.org/10.1007/s12205-021-0422-1

Yun, J. W., Kim, D. Y., Choi, B. H., Ahn, N. K., & Shim, G. Y. (2023). Performance of seismically isolated pile-supported structures through 1 g shaking table tests. *KSCE Journal of Civil Engineering, 27*(9), 3836–3847. https://doi.org/10.1007/s12205-023-0165-2

Yun, J., & Han, J. (2024). Evaluation of dynamic interactions between sloped ground and pile through centrifuge model tests. *Journal of Earthquake Engineering, 28*(4), 1069–1092. https://doi.org/10.1080/13632469.2023.2228923

Yun, J. W., & Han, J. T. (2021). Evaluation of soil spring methods for response spectrum analysis of pile-supported structures via dynamic centrifuge tests. *Soil Dynamics and Earthquake Engineering, 141*, Article 106537. https://doi.org/10.1016/j.soildyn.2020.106537

Yun, J. W., & Han, J. T. (2023). Evaluation of the dynamic behavior of pile groups considering the kinematic force of the slope using centrifuge model tests. *Soil Dynamics and Earthquake Engineering, 173*, Article 108106. https://doi.org/10.1016/j.soildyn.2023.108106

Zheng, W. Z., Wang, H., Li, J., & Shen, H. J. (2021). Parametric study of SMA-based friction pendulum system for response control of bridges under near-fault ground motions. *Journal of Earthquake Engineering, 25*(8), 1494–1512. https://doi.org/10.1080/13632469.2019.1582442